MICROSTRUCTURAL DEVELOPMENT IN HSLA-100 STEEL WELD METALS

First Annual Progress Report
Grant No. N00014-89-J-1958

Submitted by

Paul R. Howell
Associate Professor of Metals Science and Engineering
The Pennsylvania State University
University Park, PA 16802

ABSTRACT

Light microscopy, scanning electron microscopy (SEM) and transmission electron microscopy (TEM) have been employed to examine the decomposition of austenite in HSLA 100 steels. The as-received plate had been quenched and tempered and low magnification imaging suggested that the microstructure comprised lath martensite and granular bainite. However, at higher magnifications, much of the so-called granular bainite was found to consist of equiaxed ferrite which contained pools of austenite and/or martensite. The tempering treatment yielded fine dispersions of ε-Cu, within both the lath martensite and the granular bainite. Finally, the occasional observation of interphase precipitation in association with ferrite suggests that the proeutectoid ferrite reaction had initiated prior to quenching from the austenizing temperature.

For samples which had been reaustenitized and ice-water quenched, the microstructure consisted primarily of lath martensite although some "granular bainite" also observed. Slow (furnace) cooling from the austenitic range yielded an equiaxed grain structure which could be designated as granular bainite. TEM analyses revealed that the dominant reaction product in the slowly cooled steels was indeed equiaxed ferrite. This ferrite could contain pools of untransformed austenite together with martensite. Precipitation of ε-Cu occurred in the majority of the ferritic grains. The ε-Cu formed by either an interphase precipitation reaction or from supersaturated ferrite. From the observations on the as-received and furnace cooled materials, a model for the formation of granular bainite is presented.

Key words: Alloy steels,

1. INTRODUCTION

Precipitation strengthening of steel by finely dispersed copper particles has played a key role in the development of the low carbon HSLA series of steels possessing very high strength, toughness, and superior weldability. HSLA-100 alloy was developed to meet a baseline yield strength of 100 Ksi, through a quench and temper heat treatment procedure. The steel processing combines the austenite grain refining influence of niobium and the hardenability contributions from Mn, Ni, Cr and Mo to achieve a fine lath microstructure through commercial water quenching means. The quenched material is subsequently aged to provide a uniform distribution of copper precipitates while allowing for some recovery of the as-quenched microstructure. The resulting fine ferrite grain size is the principal factor contributing to the high strength - toughness combination for the HSLA-100 steel. The new steel, with its low carbon content , would permit less stringent welding and non-destructive testing procedures as well as reduce the mechanical property deterioration from welding operations.

Mechanical property evaluation of the HSLA-100 plates from the trial heat production has led The Office of Naval Research to conclude that the new steel adequately meets the requirements of strength, toughness, and nil-ductility transition characteristics. However, detailed microstructural characterization has not been carried out to:

(i) properly correlate the mechanical properties with the microstructural features, and

(ii) to provide a predictive capability to assess the response of the base metal microstructure to thermal treatments as encountered in the heat affected zone in a weldment.

This report covers the initial phase of a two-year project (Grant No: N00014-89-J-1958) to investigate the microstructural development in the ultra-low carbon HSLA-100 plate steel, weld metal, and the heat affected zones. This initial phase of the project has focussed on the analysis of the base metal microstructure and the identification of the transformation products resulting from the decomposition of austenite in the low carbon HSLA-100 steel.

Development of continuous cooling transformation (CCT) diagrams for the HSLA-100 is a major goal of this investigation. This would involve utilization of dilatometry analysis soon to be

undertaken in collaboration with DTRC. The preliminary study therefore, is aimed at identifying the austenite transformation products under extreme cooling rates that would permit the interpretation of more complex microstructures formed at intermediate cooling rates. Isothermal transformation studies carried out in parallel are expected to compliment the CCT work by facilitating proper identification of the transformation products between different temperature intervals. The microstructural analysis of the base metal would form the basis for further studies of reheat effects upon the copper precipitate dispersions as well as the influence of the heating and cooling thermal cycles as appropriate to different weld heat inputs.

2. EXPERIMENTAL APPROACH

Material samples for the present study were taken from two 1.25 inch thick plates from the trial heat production of HSLA-100 and the chemical compositions are given in Table 1. The steels are identified as GKA and GKN in keeping with the plate identification by DTRC for the physical-mechanical property characterization. The ageing heat treatment for the two steels differed slightly, and the GKA base metal analyzed in this report was solution treated at 1650°F (905°C) and water quenched prior to tempering at 1050°F (565°C) for 70 minutes followed by air cooling to room temperature. To study the effect of cooling rate on the austenite transformation products, sample material was austentized at 1000°C for 10 minutes and was either furnace cooled or oil quenched. Samples for isothermal transformation study were also solution treated at 1000°C for 10 minutes before transferring to a lead bath held at the desired temperature. On completion of the isothermal holding time, the samples were quenched in iced water.

Specimens for optical and scanning electron microscopy (SEM) were prepared using standard metallographic techniques and were etched in a mixture of 4% picral-1% nital. SEM examinations were carried out on an ISI SX 40A operated at 15 or 20 kV. Specimens for transmission electron microscopy (TEM) were prepared in a twin jet electropolisher using an electrolyte containing 5% perchloric acid (by volume) in glacial acetic acid at room temperature and at a potential of 40-50 volts. TEM was performed using a Philips EM 420 T operating at 120 kV.

3. RESULTS

3.1 Microstructure of the as-received base metal

Figure 1 shows optical and SEM micrographs of the microstructures found in the as-received base metal. The optical micrograph in figure 1a reveals regions of aligned laths as well as regions with a more equiaxed appearance. Whereas the aligned constituents can be considered to form as packets, the packet boundaries are not well revealed in this micrograph. However, the laths themselves seem to be resolved and appear to be of the order of 0.5 μm wide. Several of the adjacent laths seem to be separated either by well formed lath boundaries, delineated by etching, or by a continuous interlath phase. In other areas, the lath structure is delineated by the presence of short segments of an aligned discontinuous phase. The "granular" morphology, of the remaining region would appear to arise from the presence of dispersed second phase particles within the irregularly formed equiaxed grains of the matrix phase. The SEM micrograph in figure 1b reveals the same structure with better definition than the optical micrograph. However, the lath-like component seems to form into packets and within each packet the lath structure is apparent only by the presence of the aligned interlath constituent. SEM examination , in general, reveals that the packet boundaries are ill-defined.

The interpretation of the microstructural features in figure 1 is rather difficult. Nonetheless, it is best to review at this point some of the common terminology empolyed in the description of the features in the microstructure. The aligned or lath ferritic microstructure in the as-quenched condition may be described variously as acicular ferrite, upper bainite, or lath martensite depending on the temperature range of formation. Fast quenching of low carbon HSLA steels from the solution treatment temperature leads to a predominantly lath martensitic microstructure whereas moderate quenching of very low carbon steels, e.g., HSLA-100 can result in a mixed bainite/lath martensitic microstructure. The bainite so formed may adopt either an aligned or what has been termed a granular morphology. The "granular bainite" (Habraken and Economopoulus, 1967), unlike conventional bainite in low or medium carbon steels, is characterized by the presence of dispersed islands of austenite and martensite which are associated with "bainitic" grains. On this

basis, it is perhaps appropriate to refer to the irregularly formed ferritic microstructure with dispersed second phases in the quenched material as granular bainite although as shown later, the term ferrite may be more appropriate than banite. The granular bainite component upon aging may undergo some recovery resulting in a nearly equiaxed ferritic morphology with discrete metastable austenitic particles. Thus, the microstructure of the aged material would be predominantly tempered martensite/granular bainite. In the absence of any carbide (borne out by TEM analysis) which is commonly associated with bainite and tempered martensite, the tempered materials could be characterized as granular ferrite. Hence, in the following discussion, we shall employ the term granular bainite to describe the nearly equiaxed structure with dispersed second phases, found in the quenched material and granular ferrite to describe similar microstructures in the aged material.

In comparison to the above, preliminary microstructural characterization of the low carbon HSLA-100 by Coldren and Cox (1986) classified the microstructure in the 1.25 inch thick plate as 100% bainitic. Specifically, they examined samples taken from charpy test specimens from the 1/4 - thickness of the plate steel. Assuming that the lath and granular structures observed by Coldren and Cox corresponded to upper bainite and 'granular' bainite respectively, then the second phase particles could be cementite, martensite or islands of retained austenite. The same comment can be made regarding figures 1a, b of the present investigation. Hence, TEM analysis has been carried out to identify the microconstituents.

Figures 2a and b are representative bright field (BF) images of the lath structure, which may be classified into long parallel laths as found in lath martensite and as short laths which might be characteristic of an acicular ferritic microstructure. The elongated laths are a few microns in length, whereas the lath widths are of the order of a tenth of a micron to a few tenths of a micron. The martensitic laths are heavily dislocated (e.g., figure 1a) and the interlath boundaries are clearly revealed for the most part, and often are separated by the presence of an interlath constituent such as the short aligned particles illustrated in figure 2b. The equiaxed grains (figure 2c) are on the average 2 - 4 microns in size. Boundaries between equiaxed ferrite grains and lath structures are well defined in some cases, as in the example shown in figure 3a or are ill-defined as seen in

figure 3b where the laths seem to merge into the adjacent granular ferrite grain. This latter observation would imply that both the laths and the granular ferrite has a common origin.

The elongated interlath constituent in the microstructure is predominantly identified as retained austenite. An example of thin interlath austenitic films is shown in the centered dark field (CDF) image, formed by the (002) austenite reflection, in figure 4a. In addition. austenite particles have been found at grain boundaries and within ferritic grains. An example of an "intragranular austenite grain" is given in figure 4b. In this instance the austenite island is faceted. However, in the majority of cases the retained austenite particles exhibited more irregular morphologies.

TEM examination also revealed that ε-Cu was dispersed throughout the entire ferritic microstructure. Dispersed precipitates of ε-copper exist in a wide size range of about 2 - 30 nm. Epsilon copper precipitation may occur by heterogeneous nucleation in ferrite on dislocations and grain boundaries or by interphase precipitation at austenite/ferrite interfaces. Subsequent growth kinetics are largely dependent upon the short circuit diffusion of copper atoms along grain boundaries, dislocations and two phase interfaces. The bright field (BF) image in figure 5a shows the interaction of the precipitates with dislocations and lath boundaries. The average precipitate size is approximately 20 nm and the precipitate dispersion is fairly uniform. A second example of the distribution of of ε-copper is given in the CDF image of figure 5b. This micrograph also shows some austenitic particles in contact with the boundaries and within the ferritic matrix. While the matrix precipitation of ε-Cu yields approximately spherical particles, precipitates at grain boundaries tend to be slightly elongated as may be inferred from the CDF image in figure 5c. The elongated (rod-like) appearance is again borne out by the BF image shown in figure 5d.

Examples of very uniformly distributed, fine dispersions, less than 10 nm in size, are shown in figures 6a and b. These dispersions most probably formed from supersaturated ferrite. In addition to these matrix nucleated precipitates, there is evidence for interphase precipitation of ε-Cu (Honeycombe, 1986) . An example of interphase precipitation is given in figure 6c. Interphase precipitation of copper in steel (Ricks et. al, 1980) occurs on austenite ferrite interfaces which migrate by either a ledge or bowing mechanism (Ricks and Howell, 1983). The interphase

precipitation found in the base metal is generally associated with irregular austenite/ferrite interfaces as may be inferred from the lack of regular, planar arrays of the precipitates in figure 6c. It is also interesting to note that one of the ε-Cu precipitates (arrowed) in figure 6c is pinning the austenite/ferrite interface. In addition it should be noted that the austenite pool is wholly contained within a single ferrite grain. This point will be returned to in section 4. Since it is well known that the interphase precipitation reaction is a "high temperature transformation", its occurrence in the base plate implies that the precipitates shown in figure 6c formed prior to quenching from the original solution treatment temperature. Finally, the interphase precipitates are much coarser than those which formed from ferrite alone (e..g, compare figure 6c with figures 6a, b).

3.2 Microstructure of Continuous Cooled Material

Continuous cooled specimens have been examined to study the influence of cooling rates on the austenite decomposition products. The results presented here for the furnace cooled and the oil quenched materials are representative of the extremes in terms of the effect of cooling rates on microstructural development. Furnace cooling provided a cooling rate $\cong 0.03$ °C s^{-1} in the 800°C - 500°C range.

3.2.1 Furnace Cooled Material

The optical and SEM micrographs of figure 7a and b represent typical example of the furnace cooled specimen material. The equiaxed ferritic microstructure shows micron-sized discrete particles uniformly distributed in the matrix, along grain boundaries, and at grain corners. Hence this product might be termed granular bainite. Considering the slow cooling rates involved, some of the dark etching regions could be pearlitic and the possibility exists that some of the grain boundary phases could be cementite as has been observed in ultra-low carbon, Mn steels (Lee et. al, 1990). However, TEM examination reveals the second phase to be primarily martensitic and neither cementite nor pearlite has been observed in the slowly cooled HSLA-100 steel. Martensitic grains generally have a lath structure. However, under proper tilt conditions, several of the lath martensitic regions also reveal fine twins of the order of 10-20 nm wide as seen in figures 8a and

b. The martensitic regions have been found to be of the order of 0.5 - 5 μm in diameter and are generally associated with grain boundaries or triple junctions. Although retained austenitic particles are present, they are infrequently observed. The micron or submicron sized martensite or austenitic particles contribute to the "granular appearance" of the ferrite grains.

Copper precipitates in the slowly cooled material display a wide range of particle sizes, 10 - 50 nm, with a median particle size of about 25 nm as revealed in the micrographs in figures 9a and b. Figure 9 a also illustrates the interaction between copper precipitates and the matrix dislocations. While dislocation aided matrix precipitation is prevalent in certain grains, other grains contain interphase precipitation of copper as seen in figures 10a and b. The dispersion illustrated in figure 10a and b contains nearly planar arrays of copper precipitates (arrowed) and hence might correspond to precipitation occurring at a partially coherent austenite-ferrite interface. However, interphase precipitation was more commonly associated with curved/irregular austenite-ferrite interfaces as evidenced from the curved arrays or nearly random dispersion as found in figure 9b.

Examination of the BF-CDF pair in figure 10 suggests that only a fraction of the precipitate dispersion seen in the BF is imaged in the corresponding CDF. It is therefore, likely that interphase precipitation either adopts more than one of the possible variants of the Kurdjumov-Sachs orientation relationship or that the ferrite formed is still supersaturated in copper leading to subsequent heterogeneous precipitation. In addition to the above modes of copper precipitation, TEM analysis of the furnace cooled material also revealed a fibrous ε-Cu morphology. An example of this kind of lamellar or fibrous copper precipitation is presented in figures 11a and b. Although the crystallographic orientational restrictions of this mode of precipitation are not clearly understood, the presence of interphase precipitated copper in the same ferritic grain and of the same orientation (figure 11b) does indicate its association with a semicoherent austenite-ferrite interface. At this point, it should be noted that to the authors' knowledge, this is the first report of lamellar/fibrous Cu precipitates in steels.

3.2.2 Oil Quenched Material

Oil quenching from the solution treatment temperature (1000°C) leads to a lath martensitic/granular bainite structure as seen in fig. 12 and is very similar to the microstructures in the quarter thickness of the mill produced plates. Although the microstructure consists primarily of lath martensite, certain large martensitic regions are also seen, (figure 13) some of which reveal laths with fine twins as evident from figures 14a and b. In addition, the microstructure contains some equiaxed grains.

The dominant second phase constituent in the microstructure is retained austenite. The austenitic films are about 1 - 2 μm in length and are mostly found along interlath boundaries as seen in the CDF image in figure 15.

3.3 Microstructure of the Isothermally Transformed Material

Isothermal transformation studies are just underway and whereas a series of specimens are being examined currently, only preliminary results of samples transformed at 575°C are included in this report. Results on volume fraction estimates and percentage of product phases are deferred until detailed studies on several samples at different temperatures are complete.

The selection of 575°C for the preliminary isothermal study has been guided by the estimated transformation start temperature for the bainite (Steven and Haynes, 1980) and martensite (Andrews, 1965) reactions as well as the experimentally determined A_{c1}, for HSLA-100 (Link and Czyryca, 1988) which are listed in Table 2. Thus 575°C is expected to be midway between the ferrite and bainite C-curves. The austenite transformation for this alloy is known to be very sluggish around this temperature (Wilson et. al, 1988) and hence, we have selected transformation times of 1 hr and 5 hrs for the initial analysis.

Optical micrographs suggest that the transformed microstructure is largely "granular" like the granular features in figure 1. The transformation temperature of 575°C is well above the bainite start temperature (B_S) of 535°C and therefore, the granular structure is mostly ferritic. The untransformed austenite upon quenching should transform primarily to martensite giving rise to the

packets of lath constituents observed in the microstructure. However, morphological features in the optical/SEM micrographs are inadequate to make this distinction and therefore, volume fraction estimates of the granular ferrite component is deferred until isothermal transformation studies at lower temperatures (in the range of bainite transformation) are carried out.

TEM analysis, nonetheless, can aid in determining the nature of the granular product phase. Holding at 575°C would lead to copper precipitation in the supersaturated ferrite and therefore, it is possible to identify the granular ferrite based on the presence of copper dispersions (provided the transformation times are long enough to allow copper precipitation to reach sizes observable in the TEM). Based on this premise, TEM examination of the specimens transformed for 5 hrs at 575°C suggests that the ferrite may adopt a Widmanstaten or a granular morphology. TEM analysis also reveals that transformation of austenite to ferrite is incomplete after 5 hrs at 575°C. On quenching, the untransformed austenite is converted to martensite, which depending on the carbon enrichment may be twinned.

4. DISCUSSION

The results presented in section 3.2.2 indicate that the as-quenched microstructure of the HSLA-100 consists predominantly of lath martensite and "granular bainite". Small particles of austenite have also been identified in the microstructure. The retained austenite particles about 1micron in size display rather irregular shapes and are found at grain boundaries or within grains and in the martensite as an interlath phase.

Slow cooling rates from the austenitization temperature leads to a primarily equiaxed structure which appears to have a granular morphology. The granular appearance is mostly due to the presence of small retained austenite particles or due to small austenitic islands, enriched in carbon, that have transformed to martensite upon slow cooling. However, the occurrence of retained austenite particles is infrequent in the slowly cooled microstructure. The dominant second phase constituent in the slowly cooled microstructure is twinned martensite, and is indicative of

significant carbon enrichment of these grains from the surrounding ferrite grains. A notable result of this analysis of the slow cooled material is the absence of any pearlite or cementite.

The slowly cooled materials also contain dispersion of copper precipitates. Interphase precipitation, obeying the K-S orientation relationship (Ricks et. al, 1980), and matrix dislocation-aided precipitation from supersaturated ferrite have been identified as the principal modes of epsilon copper precipitation. However, in addition to these, the slowly cooled HSLA-100 microstructure reveals copper to precipitate in a fibrous or lamellar morphology such as found for η-Au in Fe-Ni-Au alloys (Ricks, 1981). While the atomic size mismatch has been suggested as a factor behind such fibrous precipitation in Fe-Ni-Au alloys, it is not immediately clear under what conditions such mechanisms are active in the experimental steel.

In contrast to the as-quenched material (laboratory quenched from the solution treatment temperature of 1000°C), the as-received (supposedly quenched and aged) base metal revealed the ferritic microstructure to be principally of a lath/granular structure. Retained austenite has been identified as the major second phase constituent, present as films at the interlath boundaries and as micron/sub-micron particles at grain boundaries or within the granular ferrite. The ferritic microstructure is heavily dislocated and is found to have a controlling influence on the size of the copper precipitates. Precipitation associated with the grain boundaries and dislocations tends to be much coarser compared with the uniform copper precipitation found in large equiaxed ferritic grains. Some of the large ferrite grains contained interphase copper precipitation, which conclusively suggests that the polygonal ferrite formation is not fully suppressed in the alloy. For the HSLA-100 steel with a refined ferritic microstructure, these large polygonal ferritic grains with uniformly dispersed fine precipitation may have a deleterious effect on the low-temperature brittle fracture behavior.

The formation of the granular bainite/ferrite morphology in the microstructure is not well understood (Thompson et al, 1990). However, the results of the present investigation may well provide a qualitative description of granular bainite and a mechanism for its formation. Reference to e.g., figure 1b reveals that this transformation product often consists of what would appear to be

approximately equiaxed ferrite which contains other "phases"/microconstituents. Now, reference to figures 4b, 5b and 6c shows that pools of austentite can be completely embedded in single grains of ferrite. The same is also true for martensite i.e., regions of "intragranular martensite" were also observed. Hence, it can be suggested that what has been termed "granualr bainite" is equiaxed ferrite which contains discrete pools of austenite and/or martensite. The question now becomes "What is the mechanism for the formation of intragranular pools of e.g., austenite"?

A possible sequence of events is shown in figures 16. Initially, it is assumed that sl. ape instabilities develop at the austentie/ferrite interface during ferrite formation (figure 16a). Enhanced diffusion of carbon away from the protrusions will then lead to "pinching-off" of discrete pools of austenite at the ferrite grain boundary (figure 16b).

Once the ferrite boundary has been created it is subjected to normal grain growth forces and individual boundaries will migrate towards their center of curvature. This driving force for grain growth will be counter balanced by a Zener drag force. However, if the driving force outweighs the restraining force, then the ferrite boundaries will move around the austenite particles (figure 16c) and finally break free (figure 16d). When the boundary breaks free, the austenite particle becomes embedded in the ferritic matrix. Subsequent cooling can either lead to retained austenite or it may transform to martensite. Although the above argument is somewhat speculative and little evidence for the stages shown in figures 16a-c has been presented, unambigous evidence for this sequence of events has been documented in a parallel investigation on low carbon (0.04 w/o) low alloy steels (Lee et. al, 1990).

5. CONCLUSIONS

Preliminary anlaysis of microstructural development in the 0.04 wt% carbon HSLA-100 steel leads to the following conclusions:

(i) The as-quenched microstructure consists of heavily dislocated low-carbon lath martensite and granular bainite. The principal interlath or intragranular second phase constituent is micron or sub-micron sized retained austenite.

(ii) Slow cooling from the solution treatment temperature results in a predominantly equiaxed ferritic structure (granular ferrite?). The sluggish austenite-to-ferrite transformation allows the untransformed austenite to become sufficiently enriched in carbon permitting twinned martensitic formation upon slow cooling or austenite retention.

(iii) Under very slow cooling rates, copper precipitation can take place through interphase precipitation associated with a coherent or semicoherent austenite-ferrite interface. However, additional copper precipitation from supersaturated ferrite occurs. In addition, slow cooling leads to a fibrous mode of copper precipitation.

(iv) The quenched and aged base metal contains lath and granular ferritic morphologies. The interlath constituent is generally retained austenite and is unaffected by the aging heat treatment.

(v) Precipitation of copper is significantly affected by the dislocation substructure as indicated by the increased average size of particles associated with dislocations. Grain or lath boundaries have a similar effect on precipitate size.

(vi) Isothermal transformation at 575°C for 5 hrs leads primarily to a granular microstructure. As the transformation temperature is much higher than the bainitic start temperature, the transformation product may be appropriately referred to as granular ferrite. The granular appearance arises due to the presence of small pools of retained austenite or martensite formed upon quenching from the isothermal hold temperature.

PROPOSED PLAN FOR THE SECOND YEAR

The following is a plan for the second year of this investigation.

(i) Continue the isothermal studies in progress and develop a TTT diagram after properly identifying the microstructural constituents.

(ii) Undertake continuous cooling studies at various cooling rates and utilize dilatometric techniques to establish CCT curves for the HSLA-100.

(iii) Carry out weld simulation to analyze e.g., the heat affected zone microstructure and to examine reheat effects upon the starting microstructure.

(iv) Analyze weld metal microstructures and document the influence of microalloying precipitates on the development of the microstructure.

(v) Conduct ageing studies of as-quenched material to assess copper precipitate coarsening kinetics.

REFERENCES

K. W. Andrews, JISI, pp. 721-727, 1965.

A. P. Coldren and T. B. Cox, DTNSRDC/SME-CR-07 86, 1986.

E. J. Czyryca and R. E. Link, DTRC-SME-88/62, 1988.

L. J. Habraken and M. Economopoulus in "Transformation and Hardenability in Steels" Climax-Molybdenum. Co., pp. 69-108, 1967.

R. W. K. Honecombe, Proc. Intnatl. Conf. on Phase Transformations in Ferrous Alloys, Eds., A. R. Marder and J. I. Goldstein, TMS pp 259-280, 1984.

J. W. Lee and P. R. Howell, J. Mat. Sci., Vol. 25, 1699-1710, 1990.

R. A. Ricks, and P. R. Howell, Acta Met., Vol 31, 853-861 (1983)

R. A. Ricks, P. R. Howell, and R. W. K. Honeycombe, Metal Sci., 562-568, 1980.

R. A. Ricks, J. Mat. Sci., Vol 16, 3006-3012, 1981.

W. Steven and A. G. Haynes, Atlas of Continuous Cooling Transformation Diagrams, ASM, p 228, 1980.

S. W. Thompson, D. J. Calvin, and G. Krauss, to be published.

A. D. Wilson, E. G. Hamburg, D. J. Calvin, S. W. Thompson and G. Krauss, in Microalloyed HSLA Steels, ASM, pp 259-75, 1988.

Table 1 Chemical composition of the steels (wt%)*

Steel	Alloying Element										
	C	Mn	P	S	Si	Cu	Ni	Cr	Mo	Al	Cb
GKA**	0.04	0.78	0.009	0.003	0.31	1.50	3.48	0.57	0.48	0.04	<0.05
GKN***	0.04	0.82	0.014	0.002	0.32	1.59	3.45	0.58	0.51	0.03	<0.05

*Product Analysis - DTRC (DTRC - SME - 88/62, 1988)
**Phoenix Steel Corp. Heat #56422-16, Plate #67613-01
***Lukens Steel Co., Plate #56422-16B

Cb $\simeq$ 0.03 in both steels (Ladle Analysis Phoenix)

Table 2 Critical Transformation Temperatures

$B_S \approx 535°C$ (calculated accordig to the Steven and Haynes formula)

$M_S \approx 425°C$ (calculated according to the Andrew's product formula)

$A_{C1} \approx 680°C$ (Experimental, Czyryca and Link, 1988)

B_S (°C) = 830 - 270C - 90 Mn - 37 Ni - 70 Cr - 83 Mo

M_S (°C) = 512 - 453 C - 16.9 Ni + 15 Cr - 9.5 Mo + 217 C^2 - 71.5 CxMn - 67.6 CxCr.

FIGURES CAPTIONS

Figure 1 Microstructure of the as-received HSLA-100 base metal (GKA): (a) optical and (b) SEM micrographs reveal the aligned and granular morphology.

Figure 2 TEM BF micrographs: (a) Typical heavily dislocated lath martensite, (b) Lath microstructure with short aligned interlath particles (arrowed), and (c) granular ferritic grains with second phase particles at grain boundaries and triple junction.

Figure 3 BF micrograph indicating (a) well defined lath packet boundary with adjacent polygonal ferrite grain and (b) ill-defined boundary between acicular ferritic and granular gerritic regions.

Figure 4 Centered Dark Field (CDF) images of (a) films of retained austenite and (b) austenitic particles in the granular ferritic matrix. Particle A, arrowed in (b) is faceted.

Figure 5 (a) BF image of the lath ferritic structure illustrating copper precipitate formation along dislocations and grain boundaries, (b) CDF image, formed with the austenite/copper (002) reflection, reveals uniform distribution of nearly spherical copper precipitates (the arrows indicate retained austenite), (c) Copper precipitates along lath grain boundaries (retained austenite arrowed), and (d) BF image of copper precipitates indicate a rod-like shape.

Figure 6 Uniform distribution of epsilon-copper particles in (a) equiaxed ferritic grains show a median particle size $\simeq$ 20 nm and (b) polygonal ferritic grains with a finer particle size $\simeq$ 10 nm, (c) Coarse copper precipitates formed through interphase precipitation. The large particle is retained austenite.

Figure 7 Microstructure of the slow cooled HSLA-100 (a) Optical and (b) SEM. Micrographs illustrate the equiaxed ferritic structure. Arrows indicate martensitic regions.

Figure 8 Heavily twinned martensitic grains in the slow cooled microstructure: BF micrographs show (a) very fine twins about 5 nm wide and (b) larger twins.

Figure 9 Epsilon copper precipitates in the slow cooled material: (a) BF illustrates precipitate-dislocation interaction and (b) CDF of interphase precipitated ε-copper particles shows a nearly random distribution.

Figure 10 Interphase precipitation of epsilon copper associated with a coherent/partially coherent austenite-ferrite interface: (a) BF and (b) corresponding CDF using (111) ε-copper reflection. Planar arrays of precipitates are arrowed.

Figure 11 Fibrous or lamellar mode of copper precipitates along with nearly spherical interphase precipitated copper particles (a) BF and (b) CDF (same area under different tilt conditions). Arrows indicate the initial position of the (presumably) coherent/partially coherent austenite/ferrite interface.

Figure 12 Optical micrograph of the oil-quenched microstructure - typically lath maternsitic with some granular bainite.

Figure 13 TEM BF image shows relatively large martensitic grains in the predominantly lath microstructure.

Figure 14 Large matensitic grains in the quenched material display twinned laths: (a) BF and (b) CDF using the twin reflection. Coarse ($\simeq$ 20 nm) and fine ($\simeq$ 5-10 nm) twins are visible.

Figure 15 CDF image of retained austenite found in the quenched condition. The area corresponds to the BF image in fig. 13.

Figure 16 Schematic diagram of the encapsulation of austenite by ferrite (for discussion see text).

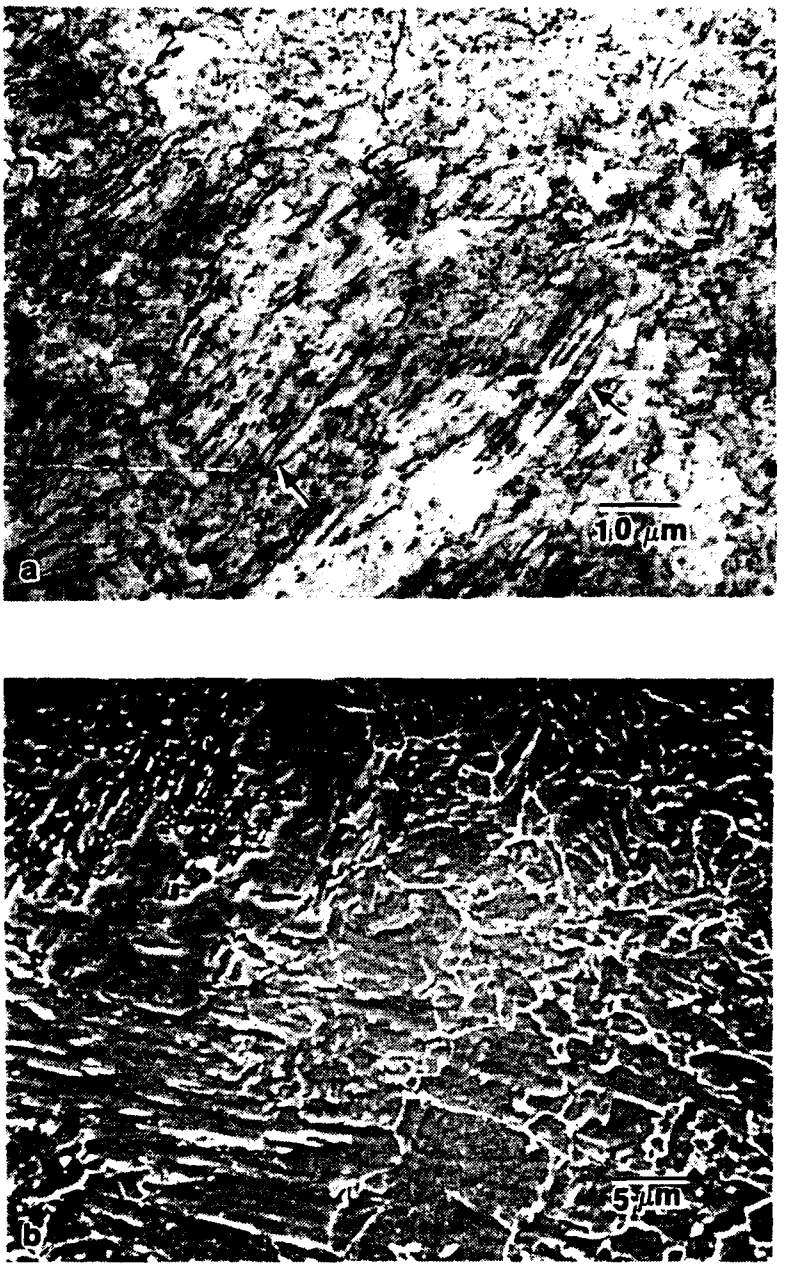

Fig. 1 Microstructure of the as-received HSLA-100 base metal (GKA): (a) optical and (b) SEM micrographs reveal the aligned and granular morphology.

Fig. 2 TEM BF micrographs: (a) Typical heavily dislocated lath martensite, (b) Lath microstructure with short aligned interlath particles (arrowed), and (c) granular ferritic grains with second phase particles at grain boundaries and triple junction.

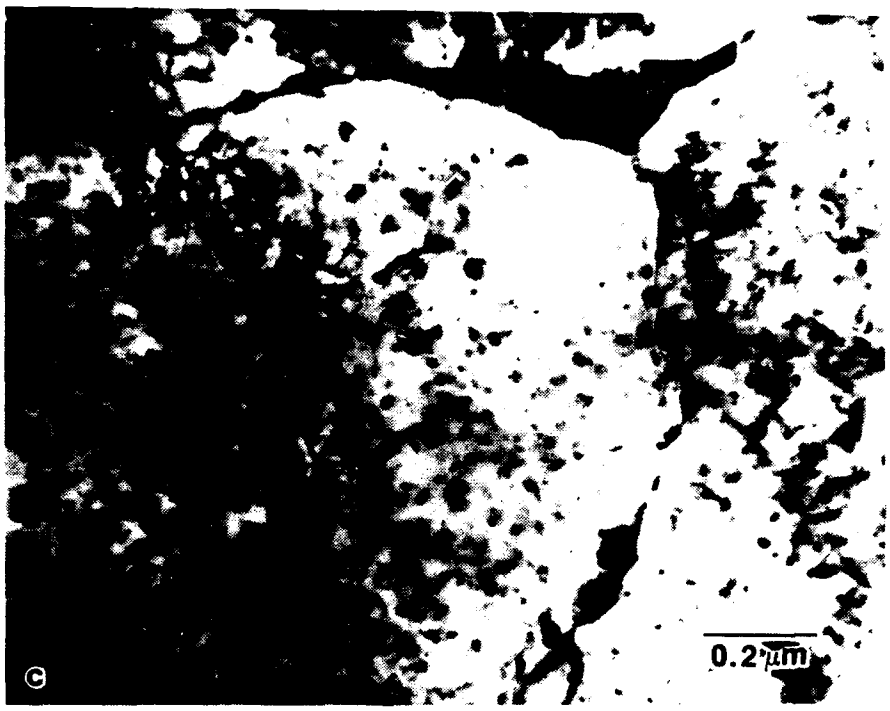
0.2 μm

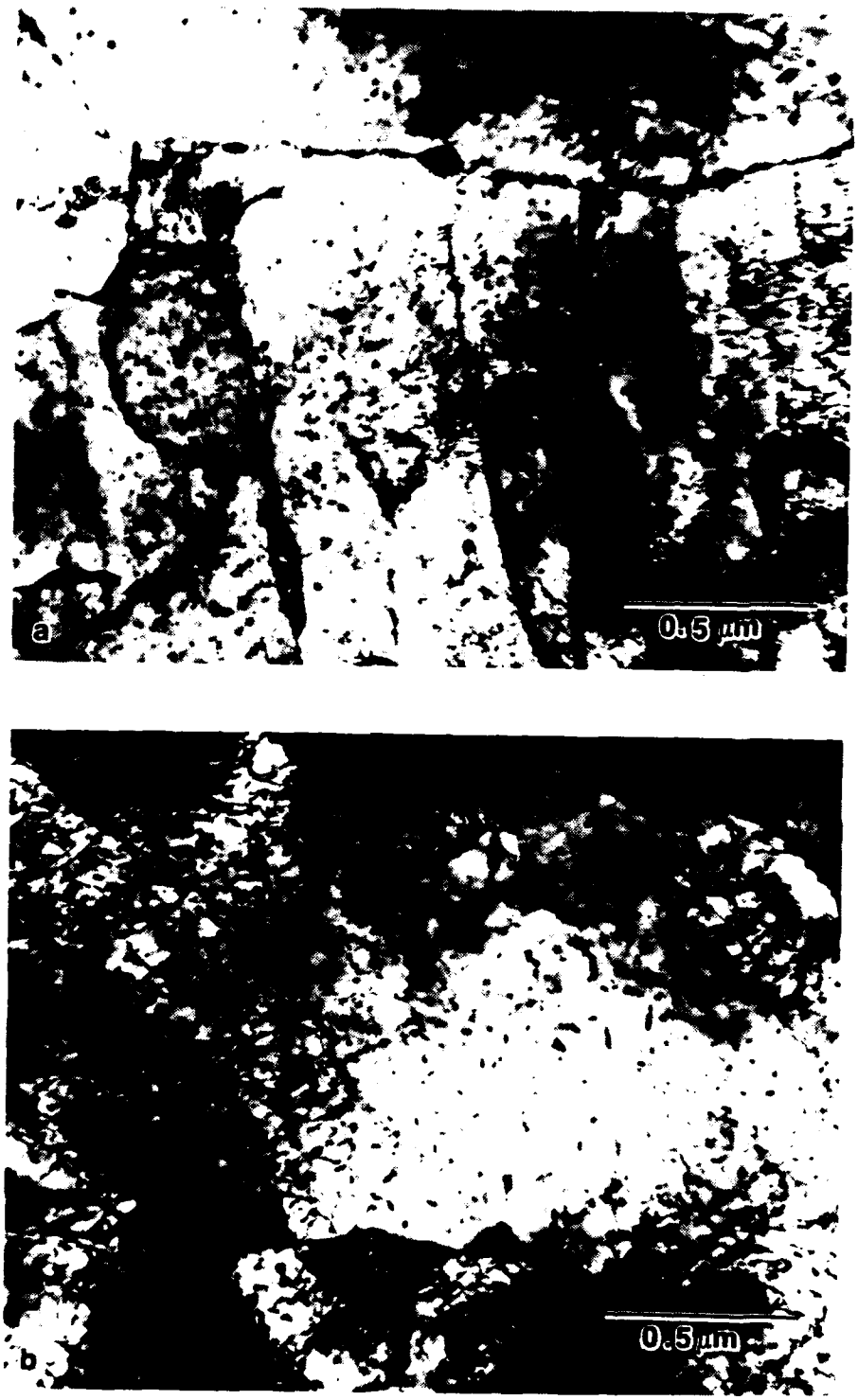

Fig. 3 BF micrograph indicating (a) well defined lath packet boundary with adjacent polygonal ferrite grain and (b) ill-defined boundary between acicular ferritic and granular gerritic regions.

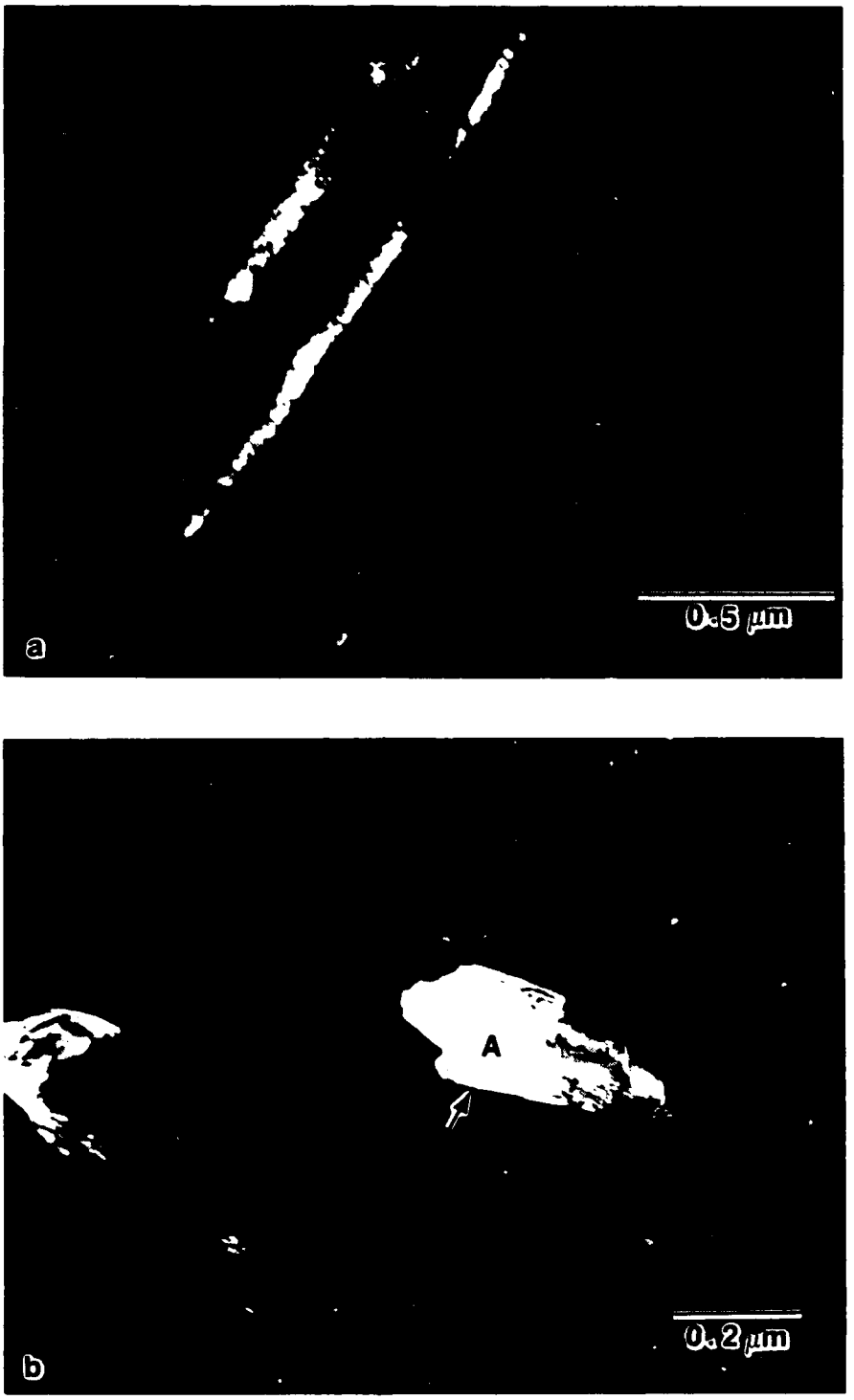

Fig. 4 Centered Dark Field (CDF) images of (a) films of retained austenite and (b) austenitic particles in the granular ferritic matrix. Particle A, arrowed in (b) is faceted.

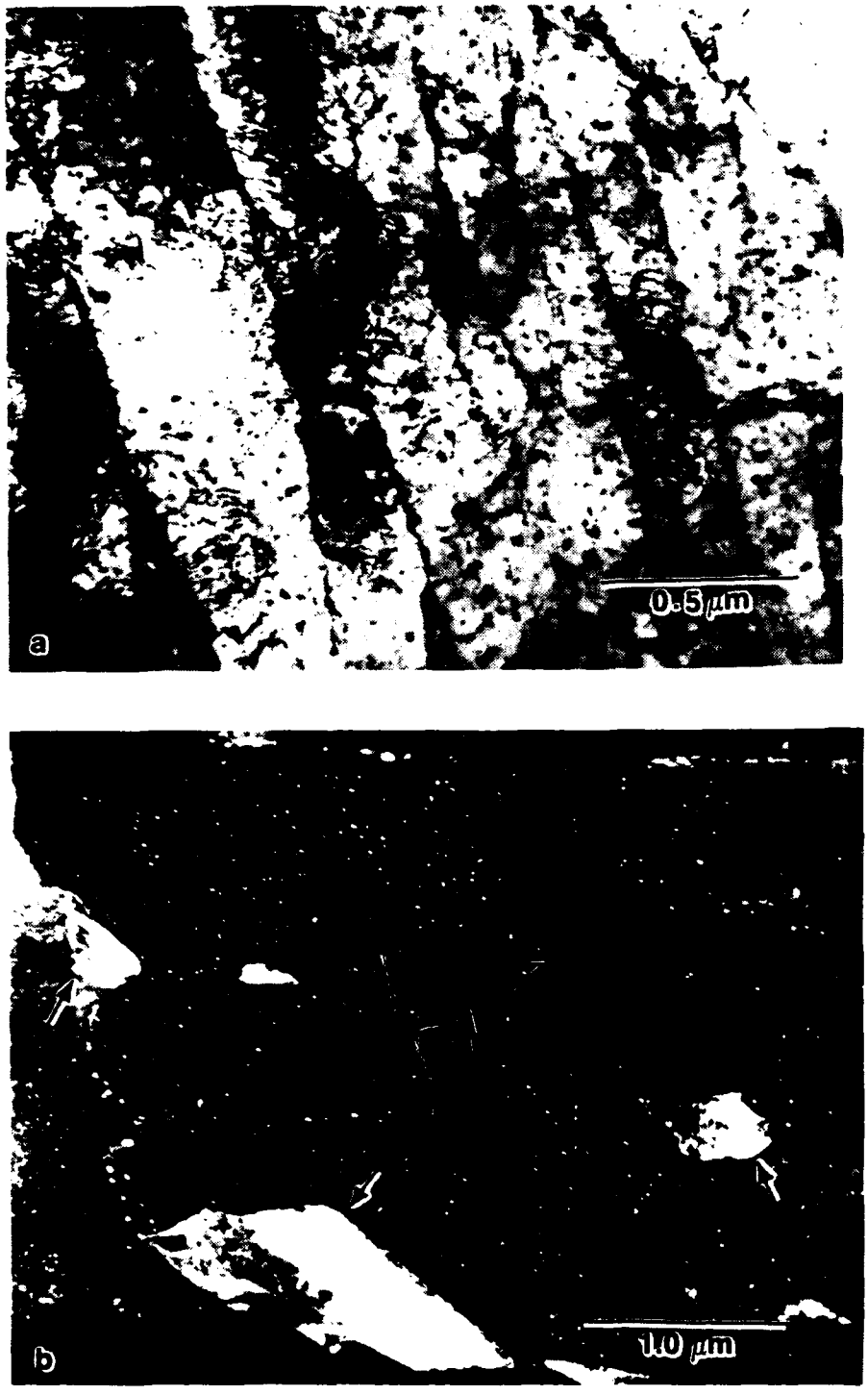

Fig. 5 (a) BF image of the lath ferritic structure illustrating copper precipitate formation along dislocations and grain boundaries, (b) CDF image, formed with the austenite/copper (002) reflection, reveals uniform distribution of nearly spherical copper precipitates (the arrows indicate retained austenite), (c) Copper precipitates along lath grain boundaries (retained austenite arrowed), and (d) BF image of copper precipitates indicate a rod-like shape.


0.5 μm
c


20nm
d

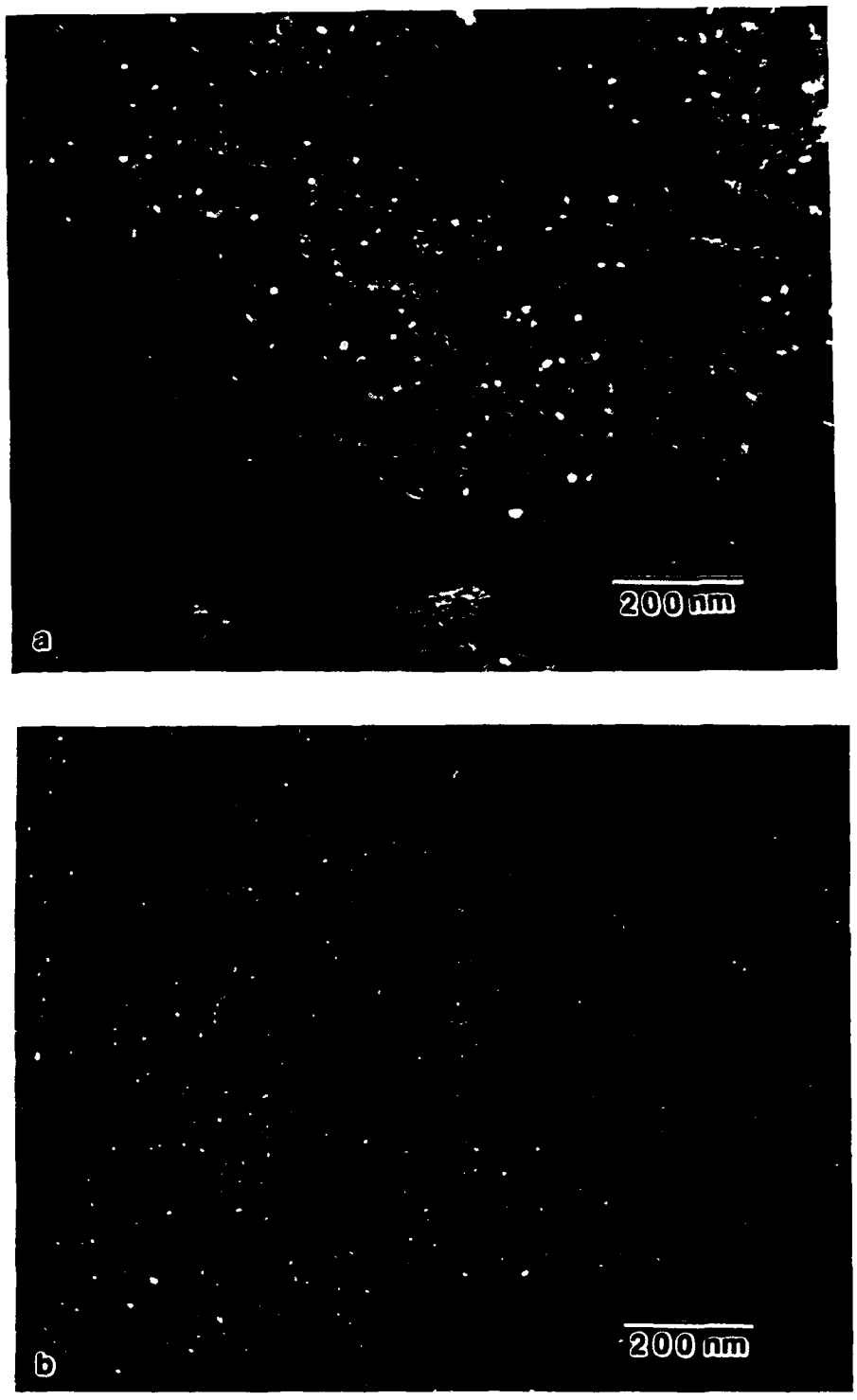

Fig. 6 Uniform distribution of epsilon-copper particles in (a) equiaxed ferritic grains show a median particle size ≃ 20 nm and (b) polygonal ferritic grains with a finer particle size ≃ 10 nm, (c) Coarse copper precipitates formed through interphase precipitation. The large particle is retained austenite.

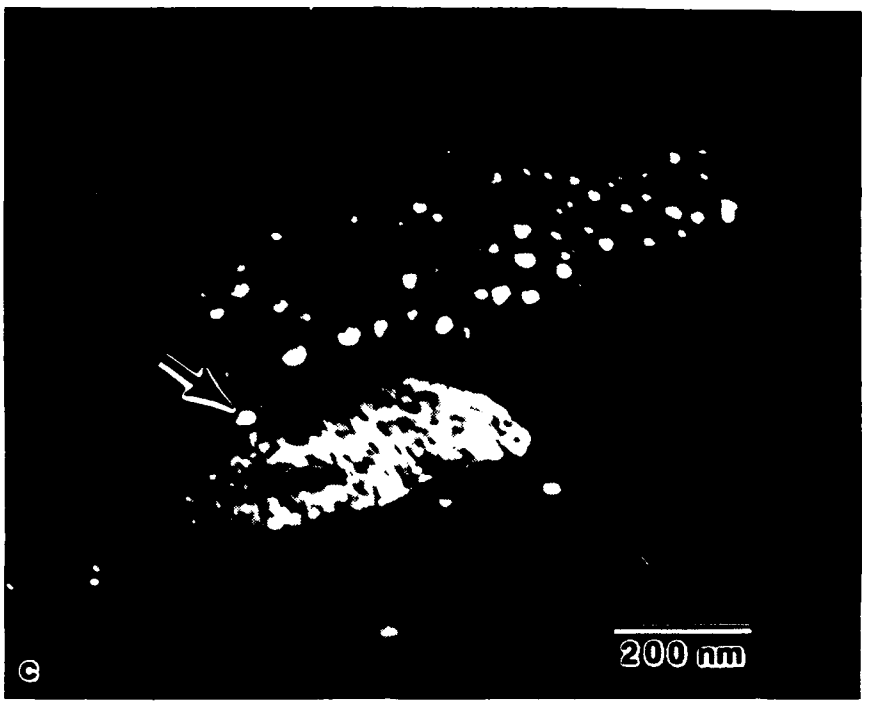
200 nm

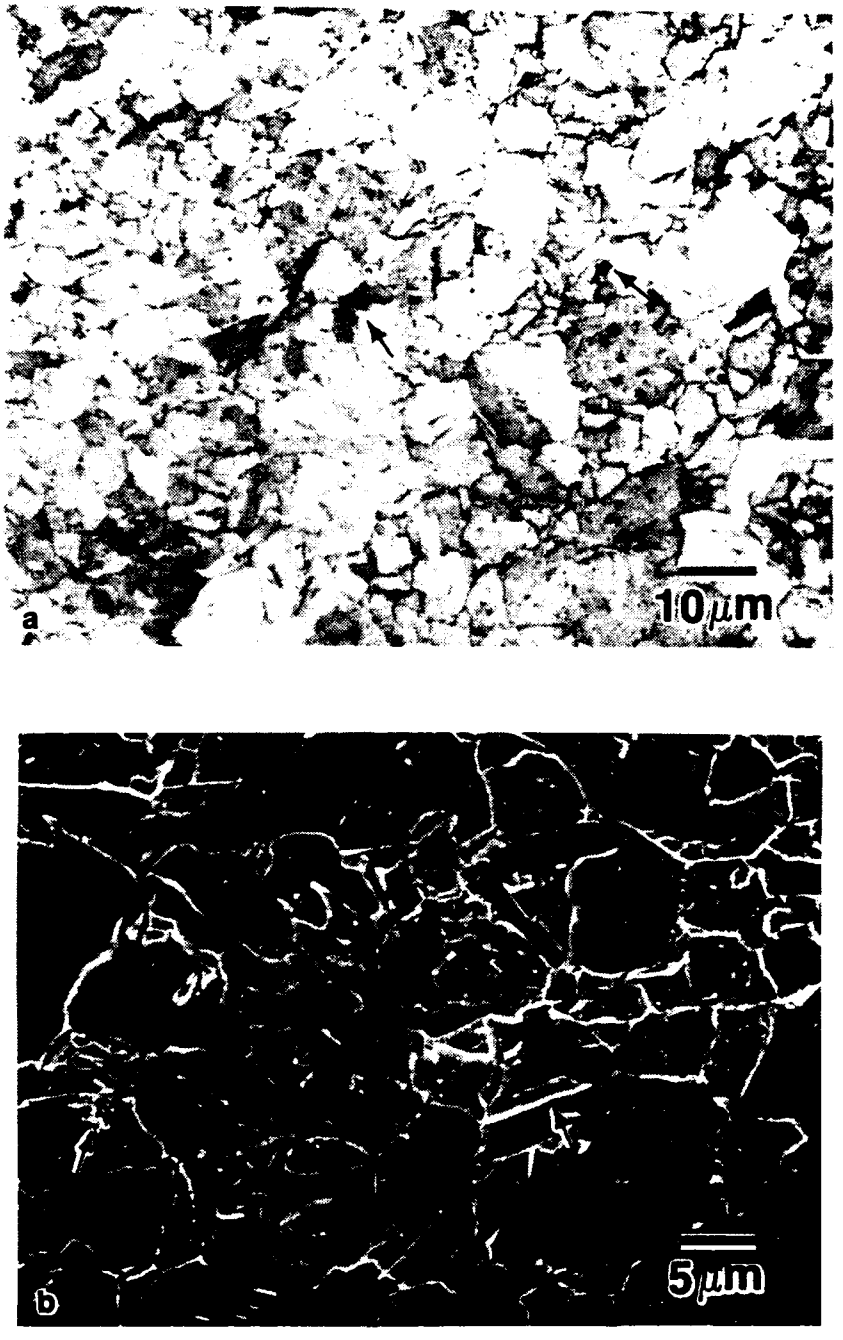

Fig. 7 Microstructure of the slow cooled HSLA-100 (a) Optical and (b) SEM. Micrographs illustrate the equiaxed ferritic structure. Arrows indicate martensitic regions.

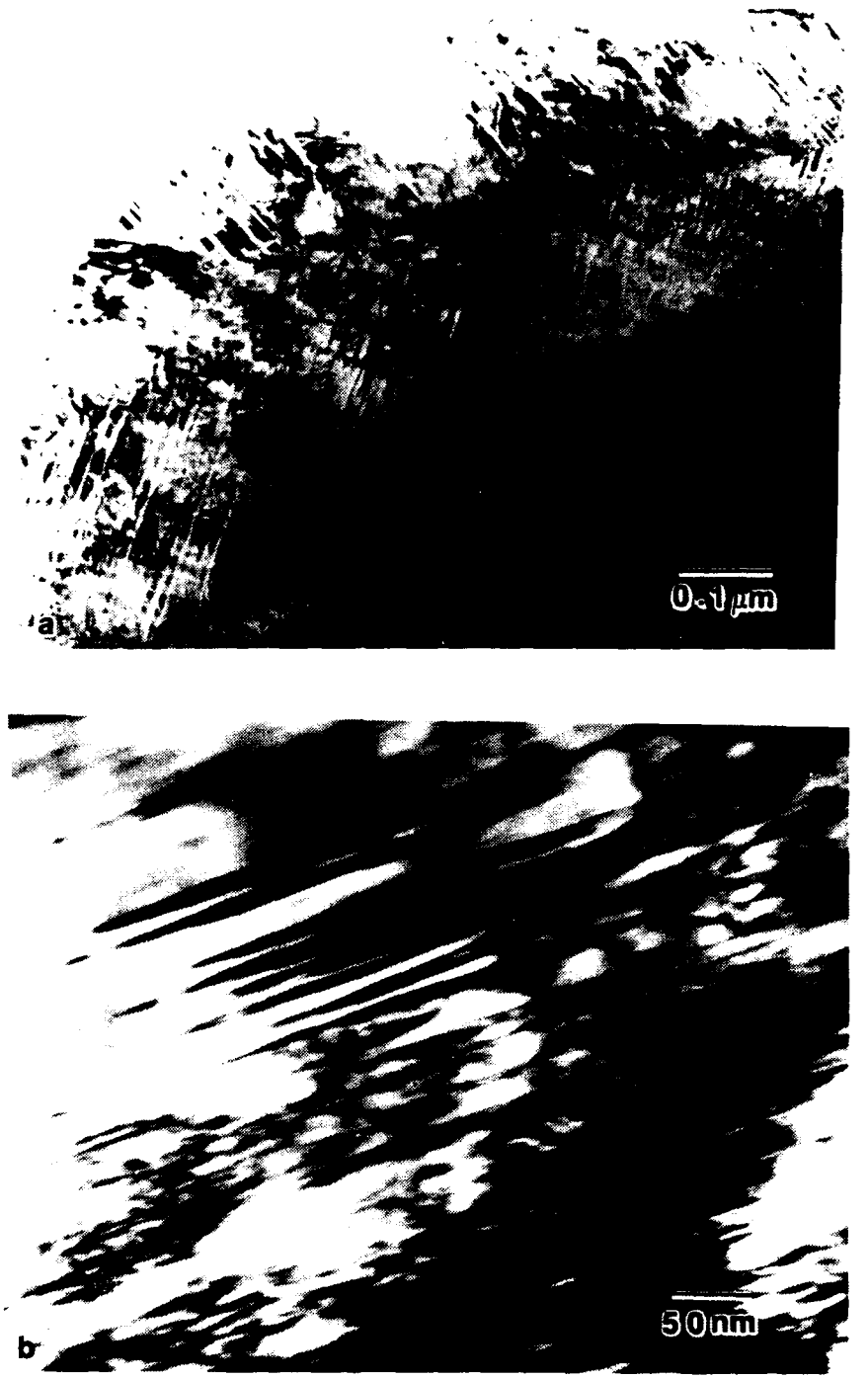

Fig. 8 Heavily twinned martensitic grains in the slow cooled microstructure: BF micrographs show (a) very fine twins about 5 nm wide and (b) larger twins.

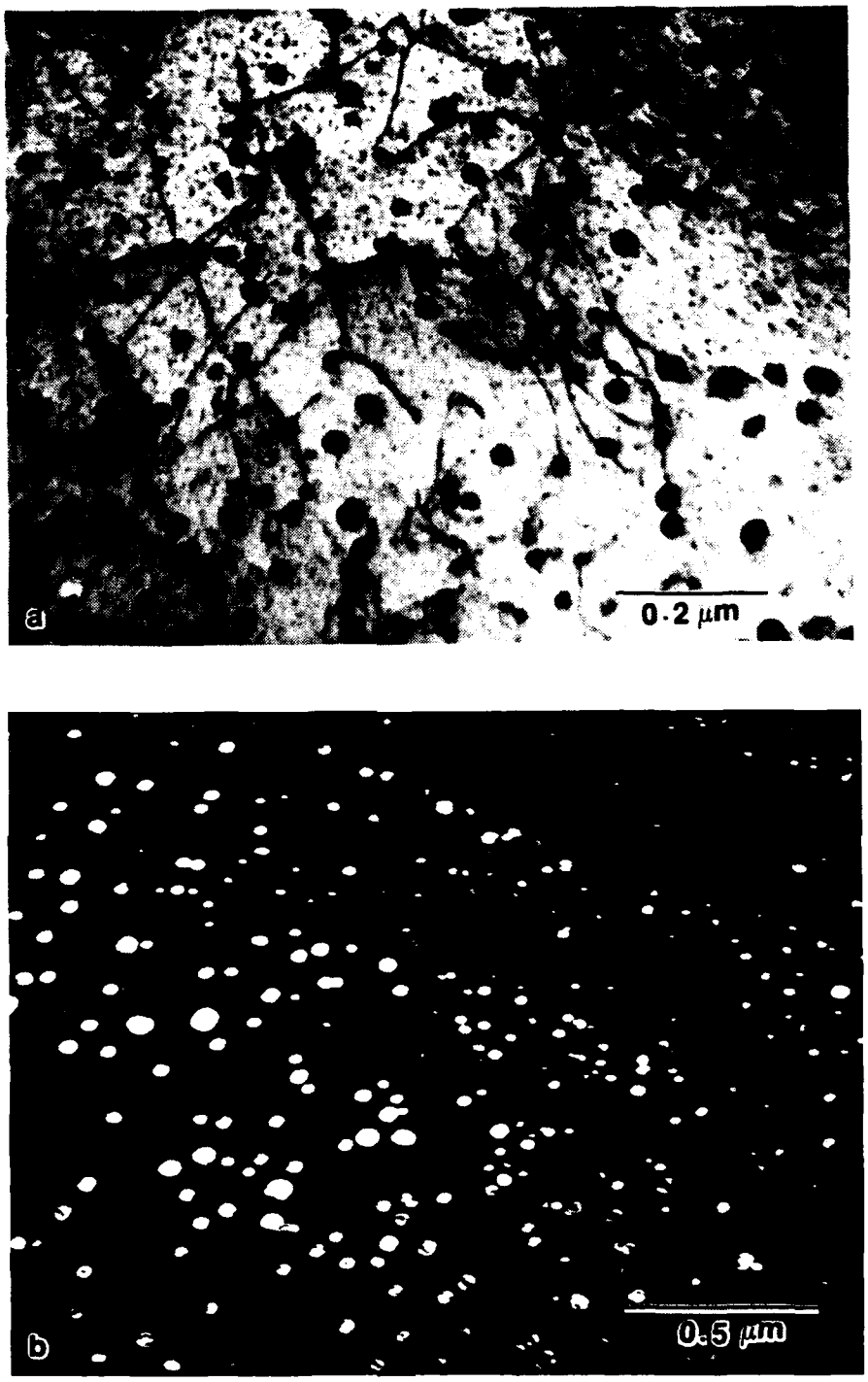

Fig. 9 Epsilon copper precipitates in the slow cooled material: (a) BF illustrates precipitate-dislocation interaction and (b) CDF of interphase precipitated ε-copper particles shows a nearly random distribution.

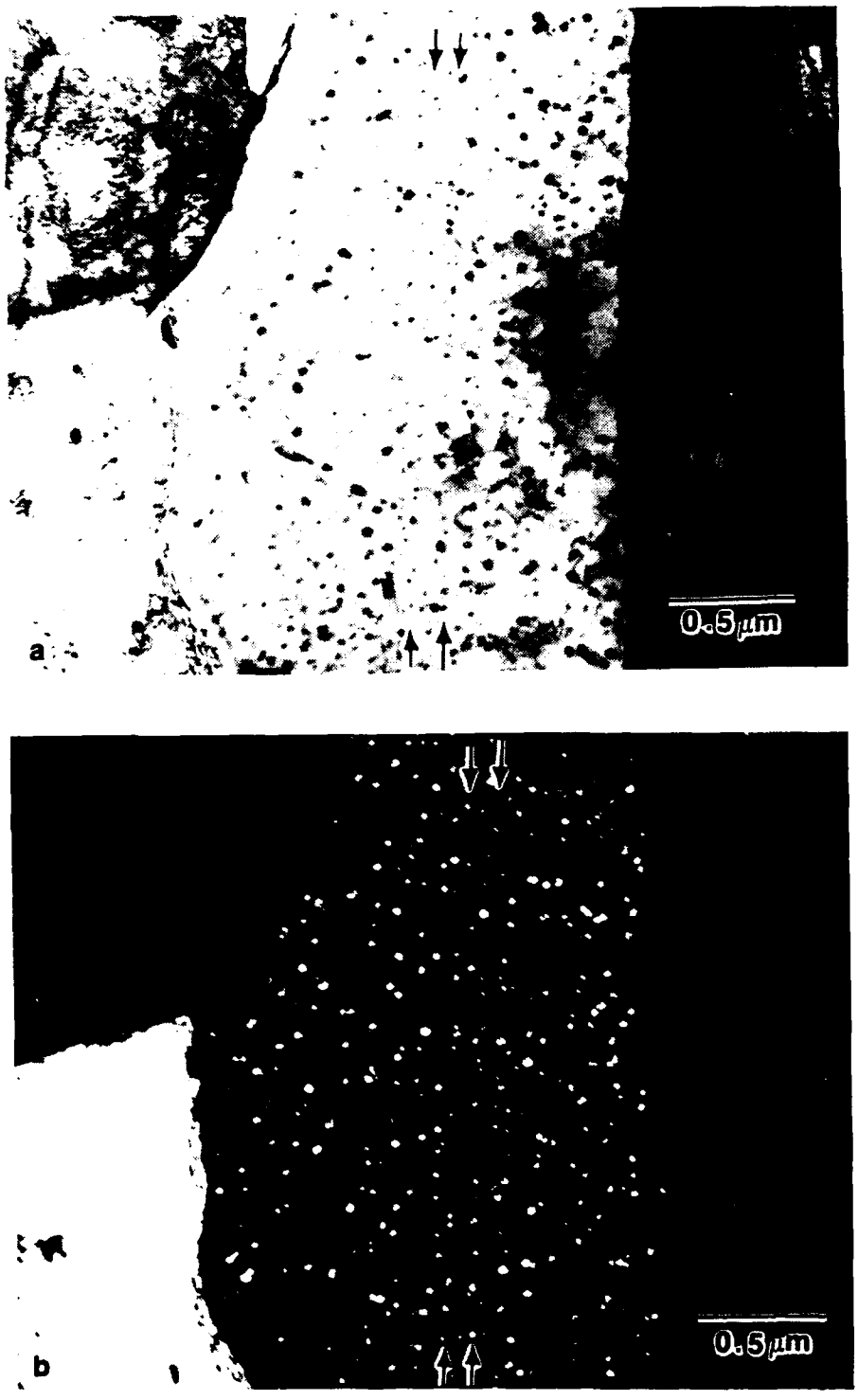

Fig. 10 Interphase precipitation of epsilon copper associated with a coherent/partially coherent austenite-ferrite interface: (a) BF and (b) corresponding CDF using (111) ε-copper reflection. Planar arrays of precipitates are arrowed.

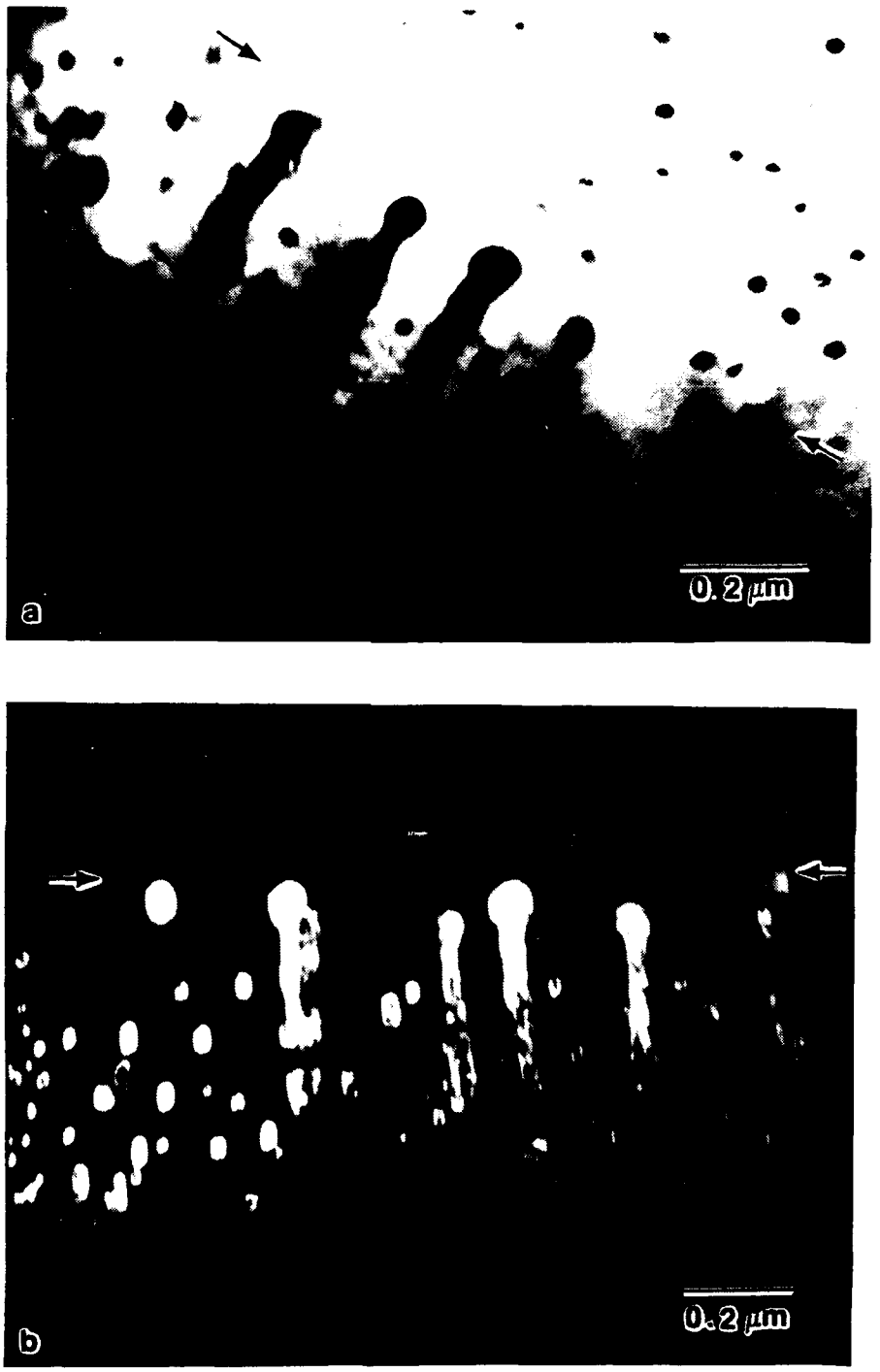

Fig. 11 Fibrous or lamellar mode of copper precipitates along with nearly spherical interphase precipitated copper particles (a) BF and (b) CDF (same area under different tilt conditions). Arrows indicate the initial position of the (presumably) coherent/partially coherent austenite/ferrite interface.

Fig. 12 Optical micrograph of the oil-quenched microstructure - typically lath matemsitic with some granular bainite.

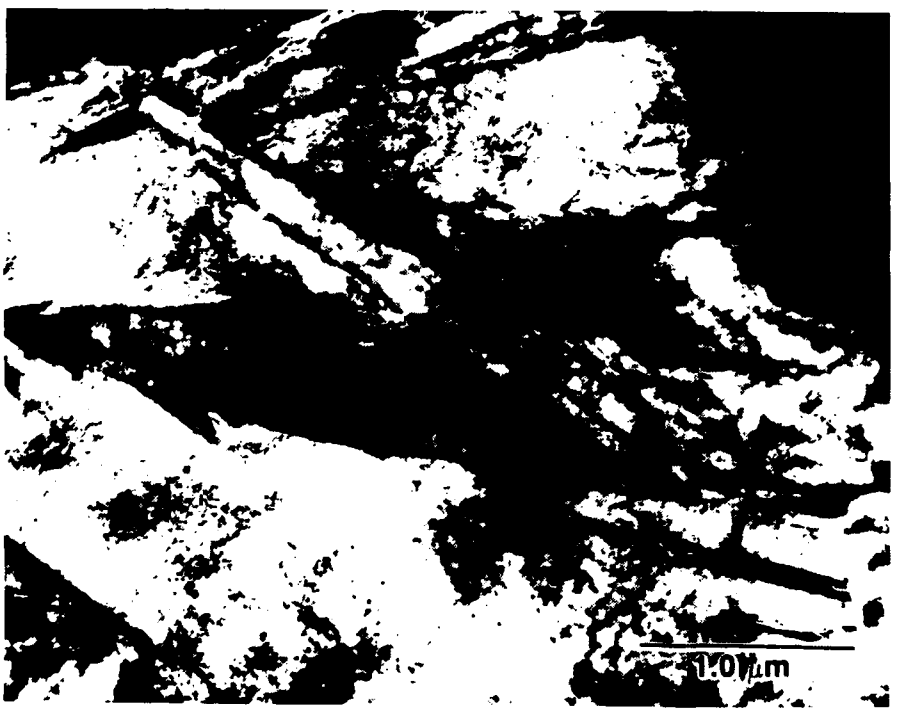

Fig. 13 TEM BF image shows relatively large martensitic grains in the predominantly lath microstructure.

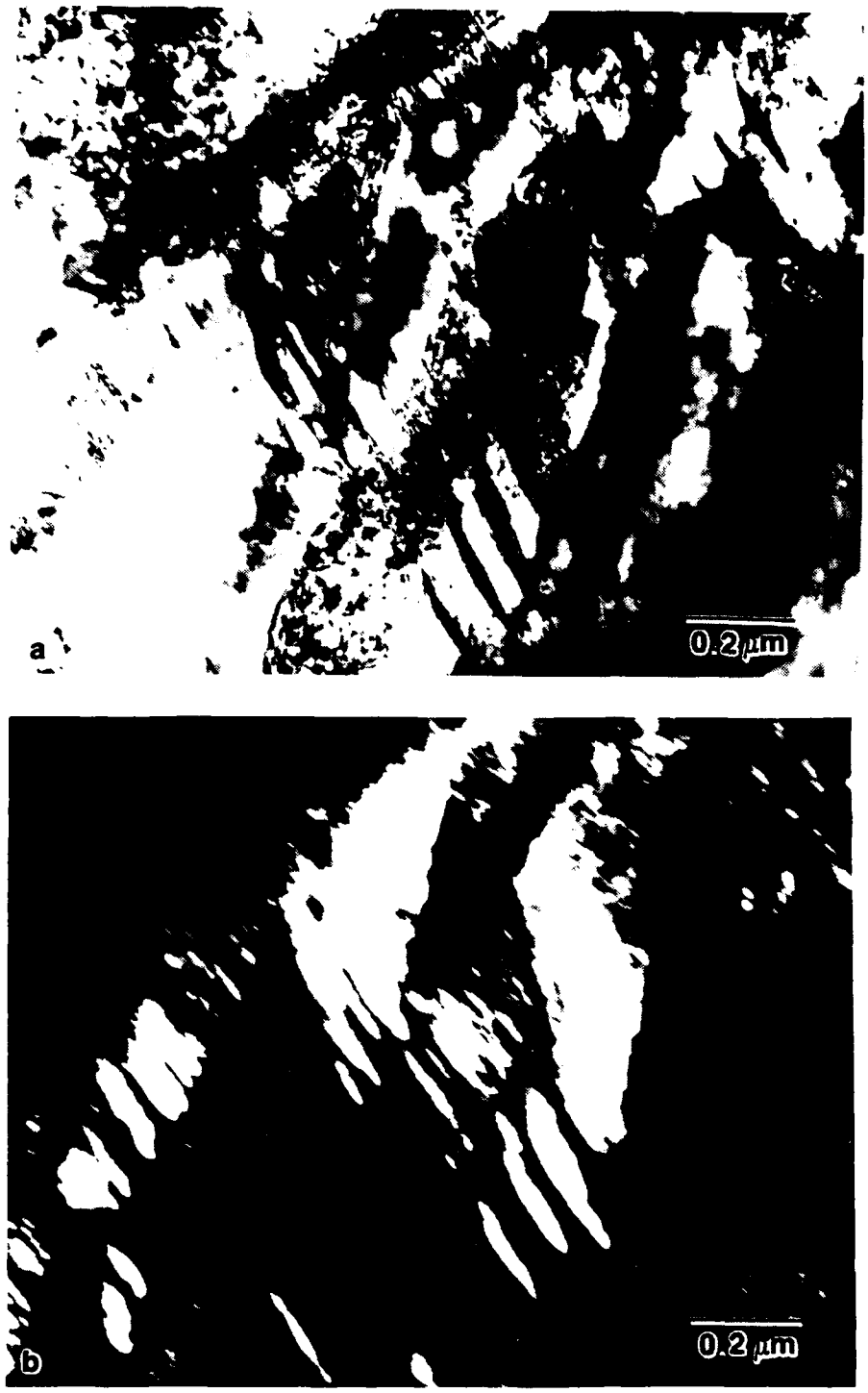

Fig. 14 Large matensitic grains in the quenched material display twinned laths: (a) BF and (b) CDF using the twin reflection. Coarse ($\simeq$ 20 nm) and fine ($\simeq$ 5-10 nm) twins are visible.

Fig. 15. CDF image of retained austenite found in the quenched condition. The area corresponds to the BF image in fig. 13.

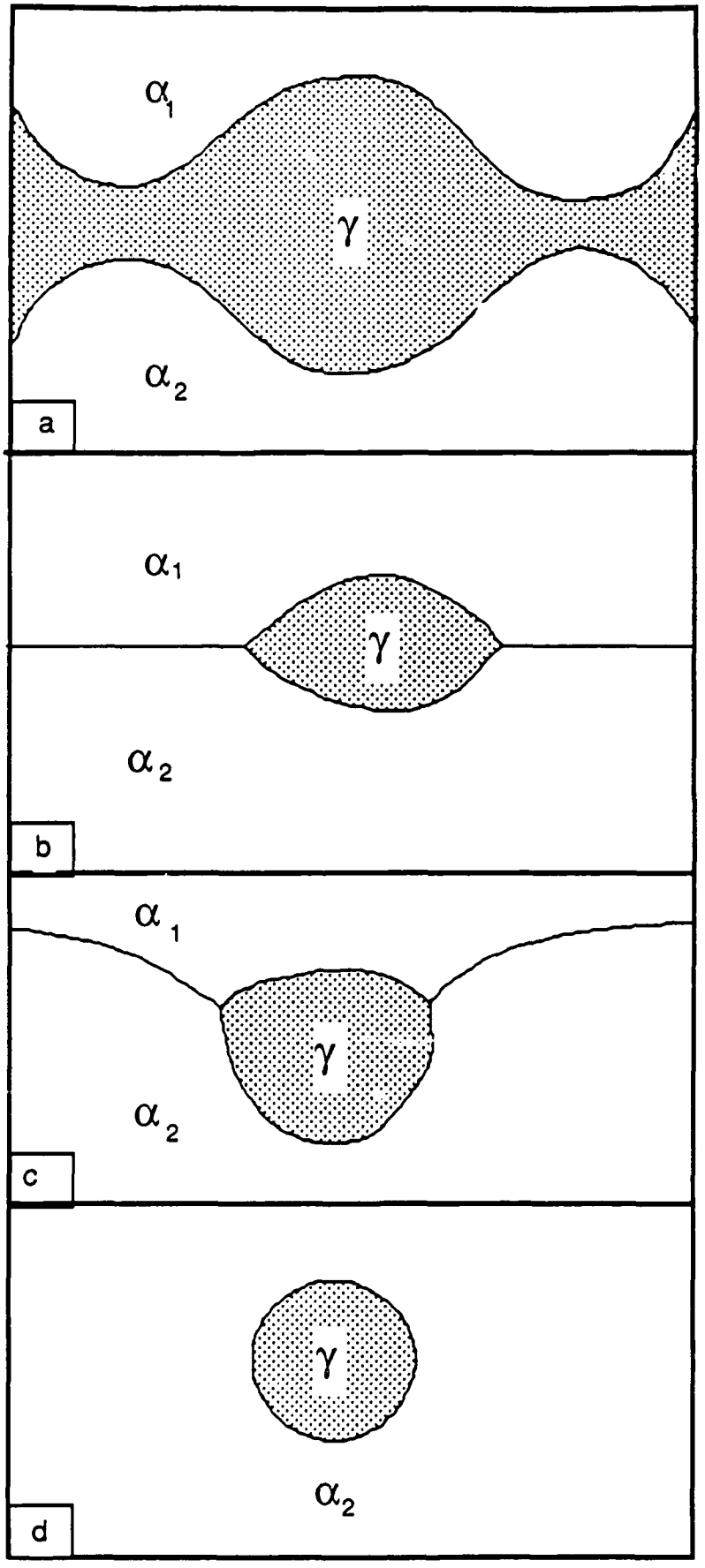

Figure 16 Schematic diagram of the encapsulation of austenite by ferrite (for discussion see text).